

Theory of biexcitons and biexciton-exciton cascade in graphene quantum dotsIsil Ozfidan,^{1,2} Marek Korkusinski,¹ and Pawel Hawrylak^{1,2}¹*Quantum Theory Group, Security and Disruptive Technologies, Emerging Technologies Division,
National Research Council of Canada, Ottawa, Canada K1A 0R6*²*Physics Department, University of Ottawa, Ottawa, Canada*

(Received 22 November 2014; revised manuscript received 27 February 2015; published 24 March 2015)

We present a microscopic theory of biexcitons in colloidal graphene quantum dots, and we discuss the possibility of a biexciton-exciton cascade generation. Assuming a p_z orbital on each carbon atom, the single-particle properties are described in the tight-binding model. The screened direct, exchange, and scattering matrix elements of the Coulomb matrix are calculated using Slater p_z orbitals. The many-body ground and excited states are constructed as a linear combination of a finite number of electron-hole pair excitations from the Hartree-Fock ground state by exact diagonalization techniques. The exciton and biexciton states are constructed exploiting the degeneracy of the valence- and conduction-band edges. The two degenerate exciton (X) states and a corresponding biexciton (XX) state are identified for generation of the XX - X cascade in threefold-symmetric quantum dots. Finally, the Auger coupling of the XX state with the excited X states is predicted.

DOI: [10.1103/PhysRevB.91.115314](https://doi.org/10.1103/PhysRevB.91.115314)

PACS number(s): 78.67.Wj, 81.05.ue, 73.22.Pr, 31.15.xr

I. INTRODUCTION

There is currently interest in the size, shape, edge, layer, and carrier density engineering of graphene [1–20], including its interesting optical [21–26] and electronic [27–36] properties. The generation and stability of biexcitons in carbon nanotubes as well as conjugated polymers have been studied extensively both theoretically and experimentally [37–46], while investigation of biexcitons in graphene quantum dots is beginning to attract attention [47,48].

The opening of an energy gap due to size quantization in graphene quantum dots [21–36,49–57] makes graphene, a semimetal, similar to semiconductor quantum dots but with small spin-orbit coupling. Strong spin-orbit coupling in semiconductor quantum dots is responsible for the existence of two degenerate interband optical transitions and, at first glance, two degenerate exciton states. The cascade between a biexciton and two degenerate exciton levels in semiconductor quantum dots has been proposed as a method for the generation of entangled photon pairs [58–61]. However, it became clear that the degeneracy of the two exciton levels is removed by electron-hole anisotropic exchange interaction [62–69] destroying photon entanglement. On the other hand, the advantage of using semiconductor quantum dots is the existence of a well-defined, unique biexciton state.

By contrast, graphene quantum dots [70] shown in Fig. 1(a) exhibit robust, degenerate exciton states and could potentially replace semiconductors in entangled photon generation if a well-defined biexciton level could be found. The two degenerate, bright exciton states, separated from the band of optically dark excitations, are a result of the degenerate valence- and conduction-band edge [Fig. 1(b)], a consequence of C_3 symmetry of these graphene quantum dots.

Here we present a theory of biexcitons in graphene quantum dots. We use a combination of a tight-binding (TB) method for one-electron states expanded in orthogonal p_z orbitals localized on each carbon atom, a self-consistent-Hartree-Fock (HF) method to determine the ground state of a half-filled, charge-neutral quantum dot, and, lastly, a configuration-interaction (CI) method to determine the band of low-energy

biexcitons. This allows us to identify a biexciton state as a candidate for the XX - X cascade and determine its Auger lifetime due to coupling with excited exciton states.

The paper is organized as follows. In Sec. II we describe the model Hamiltonian, the multiexciton CI method, and optical selection rules. In Sec. III we examine, in detail, the band-edge excitons and biexcitons. In Sec. IV we discuss our numerically obtained biexciton spectrum, elaborate on its convergence and the Auger processes, and discuss the XX - X cascade. Finally, Sec. V contains our conclusions.

II. THE MODEL

In this work, we focus on colloidal graphene quantum dots (CGQDs) with triple-axis rotational symmetry (C_3), which results in degenerate band edges responsible for the existence of degenerate, bright exciton states as discussed previously [70]. The C_3 class includes not only previously studied C168 colloidal GQDs [70–76] but also triangles, hexagons, stars, and other structures shown in Figs. 1(a) and 1(c). In this paper, we concentrate on the C168 CGQD; however, one expects qualitatively similar results for any graphene quantum dot belonging to the C_3 class.

C168 is modeled as a two-dimensional cluster of carbon atoms, depicted in Fig. 1(c), forming a finite honeycomb lattice with bond length $a_0 = 0.142$ nm. We assume that mobile electrons occupy the orthogonal atomic p_z orbitals, $|j\rangle$, located on each carbon atom j , and the remaining electrons are strongly bound forming the bonds in the plane of the CGQD and partially shielding the Coulomb potential of the carbon nucleus [24,25,35,54,56,70]. As a result, the charge-neutral CGQD with N atoms carries N mobile electrons.

Following our previous work [70], we start with the tight-binding (TB) Hamiltonian, $H_{\text{TB}} = \sum \tau_{jl} c_{j\sigma}^+ c_{l\sigma}$, where $c_{j\sigma}^+$ ($c_{j\sigma}$) creates (annihilates) an electron on orbital j , and τ_{jl} is the effective hopping term. The hopping term, restricted to include nearest-neighbor (NN) and next-nearest-neighbor (NNN) tunneling only, involves scattering from the positive background, and thus is different for the edge and interior atoms of the CGQD.

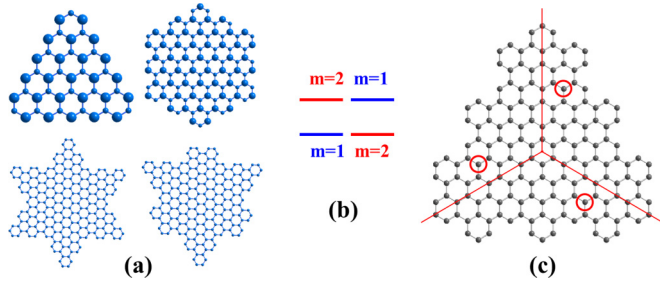


FIG. 1. (Color online) (a) Graphene quantum dots with C_3 symmetry, (b) the characteristic degenerate band edge of C_3 -symmetric GQDs, (c) the C168 structure depicting the symmetry mapped segments. The carbon atoms, equivalent by the triple-axis symmetry, are circled in red.

Using triple-axis symmetry, we can rotate the tight-binding Hamiltonian to diagonalize it into blocks labeled by different angular momenta projections $m = \{0, 1, 2\}$ or equivalently $m = \{0, 1, -1\}$. The rotation is done by selecting atom j in segment $\beta = 0$ and obtaining the equivalent atoms in segments $\beta = \{1, 2\}$ by rotating the atom “ j ” in section $\beta = 0$, as depicted in Fig. 1(c). As a result, j will now count over the $N/3$ orbitals, contained within one segment, and $\beta = \{0, 1, 2\}$ counts over segments. Connecting them by a phase $e^{i\beta m 2\pi/3}$, where β is determined by the segment from which the orbital is taken, the three orbitals $|j, \beta\rangle$ are now rotated to [70,77]

$$\Psi_j^m = \frac{1}{\sqrt{3}} \sum_{\beta=0}^2 e^{i\beta m 2\pi/3} |j, \beta\rangle. \quad (1)$$

After obtaining the blocks through the rotation of basis defined in Eq. (1), each m -block is diagonalized to give single-particle levels $|\hat{i}_m\rangle = \sum_j A_j^i \Psi_j^m$, with energies $\varepsilon_{\hat{i}_m}$, labeled by the angular momentum m .

Next, we account for electron-electron interactions. In a localized basis, the screened electron-electron interactions are described by the Coulomb matrix elements

$$\langle ij|V|kl\rangle = \iint d\mathbf{r}_1 d\mathbf{r}_2 \psi_i^*(\mathbf{r}_1) \psi_j^*(\mathbf{r}_2) \times \frac{e^2}{\kappa |\mathbf{r}_2 - \mathbf{r}_1|} \psi_k(\mathbf{r}_2) \psi_l(\mathbf{r}_1), \quad (2)$$

where $\psi_i(\mathbf{r})$ represents p_z orbitals localized on atom i approximated by Slater functions [70]. In calculating Coulomb matrix elements, we approximate the orthogonal tight-binding wave functions by nonorthogonal Slater orbitals following the Lowdin orthogonalization procedure, and we neglect contributions from overlap matrix elements [78]. All direct, exchange, and scattering Coulomb matrix elements for up to second-nearest-neighbor atoms are calculated using Eq. (2), while for atomic separations greater than NNN the matrix elements are approximated by classical point-charge interactions [24,25,35,54,56]. Coulomb interactions are assumed to be screened by the effective dielectric constant κ , which includes contributions from both the σ electrons of graphene and from the solvent in which the CGQDs are suspended.

The interacting Hamiltonian is written as

$$\begin{aligned} \hat{H}_{\text{QD}} = & \sum_{\hat{i}_m \sigma} \varepsilon_{\hat{i}_m \sigma} c_{\hat{i}_m \sigma}^+ c_{\hat{i}_m \sigma} \\ & + \frac{1}{2} \sum_{\hat{i}_m \hat{j}_n \hat{k}_p \hat{l}_q \sigma \sigma'} \delta_{m+n, p+q} \langle \hat{i}_m \hat{j}_n | V | \hat{k}_p \hat{l}_q \rangle \\ & \times c_{\hat{i}_m \sigma}^+ c_{\hat{j}_n \sigma'}^+ c_{\hat{k}_p \sigma'} c_{\hat{l}_q \sigma}, \end{aligned} \quad (3)$$

where $c_{\hat{i}_m \sigma}^+$ ($c_{\hat{i}_m \sigma}$) are the electron creation (annihilation) operators on states $|\hat{i}_m\rangle$ with angular momentum m and spin σ .

The Coulomb matrix elements in Eq. (3) are rotated from the lattice site representation, as in Eq. (2), to the $|\hat{i}_m\rangle$ basis. The Coulomb interactions conserve the total angular momentum, which can be demonstrated by collecting all phase terms $e^{i(\beta m + \alpha n - \gamma p - \theta q)2\pi/3} \langle ij|V|kl\rangle$ with the same set of $\{\beta, \alpha, \gamma, \theta\}$, and showing that the sum of their coefficients becomes zero unless $m + n = p + q$.

A. Hartree-Fock approximation

Since the full interacting Hamiltonian for the 168-atom CGQD cannot be diagonalized exactly, we start with the Hartree-Fock (HF) approximation. The mean-field HF Hamiltonian, H_{MF} , is obtained from the full Hamiltonian by replacing the two-body scattering terms by those describing scattering of a single quasielectron by the mean Coulomb potential of all other electrons. This Hamiltonian is

$$\begin{aligned} H_{\text{MF}} = & \sum_{\hat{i}_m \sigma} \varepsilon_{\hat{i}_m \sigma} c_{\hat{i}_m \sigma}^+ c_{\hat{i}_m \sigma} + \sum_{\hat{i}_m \hat{j}_n \hat{k}_p \hat{l}_q \sigma \sigma'} \rho_{\hat{j}_n \hat{k}_p \sigma'} c_{\hat{i}_m \sigma}^+ c_{\hat{l}_q \sigma} \\ & \times (V_{\hat{i}_m \hat{j}_n \hat{k}_p \hat{l}_q} - V_{\hat{i}_m \hat{j}_n \hat{l}_q \hat{k}_p} \delta_{\sigma \sigma'}), \end{aligned}$$

where $\rho_{\hat{j}_n \hat{k}_p \sigma'} = \langle c_{\hat{j}_n \sigma'}^+ c_{\hat{k}_p \sigma'} \rangle$ are the elements of the density matrix, and the Coulomb term is contracted as $V_{\hat{i}_m \hat{j}_n \hat{k}_p \hat{l}_q} = \langle \hat{i}_m \hat{j}_n | V | \hat{k}_p \hat{l}_q \rangle$.

We rotate our basis from single-particle eigenstates $|\hat{i}_m\rangle$ into a HF quasiparticle basis $|r_m\rangle$, denoting new creation (annihilation) operators on the HF states as $b_{r_m \sigma}^+$ ($b_{r_m \sigma}$). The HF states are also labeled by the angular momentum. These operators can be written as linear combinations of operators in an atomic (localized) basis, $b_{r_m \sigma}^+ = \sum_{i=1}^N B_{r_m, i} c_{i \sigma}^+$. The above rotation to HF quasiparticle states is done self-consistently until a convergence is reached for the HF ground-state energy. The resulting HF energies, ε_{r_m} , are composed of single-particle energies and self-energies accounting for all direct and exchange interactions of the electron on orbital r_m with all other electrons that fill up the valence band. On the basis of the HF orbitals, at convergence, the HF Hamiltonian is diagonal: $H_{\text{MF}} = \sum_{r_m, \sigma} \varepsilon_{r_m \sigma} b_{r_m \sigma}^+ b_{r_m \sigma}$.

B. Correlations and multipair excitations relations

We now account for electron-electron interactions beyond the Hartree-Fock approximation. We start by rewriting the full

interacting Hamiltonian, H_{QD} , in the HF basis [70],

$$H_{\text{QD}} = \sum_{r_m \sigma} \epsilon_{r_m \sigma} b_{r_m \sigma}^+ b_{r_m \sigma} + \frac{1}{2} \sum_{r_m s_n t_p z_q \sigma \sigma'}^N \delta_{m+n, p+q} \langle r_m s_n | V_{\text{HF}} | t_p z_q \rangle \times b_{r_m \sigma}^+ b_{s_n \sigma'}^+ b_{t_p \sigma} b_{z_q \sigma} - \sum_{r_m s_n \sigma} V_{r_m s_n \sigma}^{\text{MF}} b_{r_m \sigma}^+ b_{s_n \sigma}. \quad (4)$$

The interaction between HF quasiparticles is now measured with respect to the mean-field interaction term V_{HF} , already included in the self-energy contribution to ϵ_{r_m} [70].

Electronic correlations are included as interactions of HF quasiparticles through the configuration-interaction (CI) method. The CI Hamiltonian is constructed by writing Eq. (4) in the basis $\{|\text{HF}_{\text{GS}}\rangle, |X_{r_m s_n}\rangle, |XX_{r_m s_n t_p z_q}\rangle, \dots\}$, which includes the HF ground state and up to a selected number of excitations labeled by the total projection of spin, $|X_{r_m s_n}\rangle = b_{r_m \sigma}^+ b_{s_n \sigma} |\text{HF}_{\text{GS}}\rangle$, $|XX_{r_m s_n t_p z_q}\rangle = b_{r_m \sigma_1}^+ b_{s_n \sigma_2}^+ b_{t_p \sigma_1} b_{z_q \sigma_2} |\text{HF}_{\text{GS}}\rangle$, and so on. The CI Hamiltonian is then diagonalized numerically to obtain the correlated eigenstates, $|\Phi_\nu\rangle$, of the form

$$|\Phi_\nu\rangle = k_0^\nu |\text{HF}_{\text{GS}}\rangle + \sum_{r_m s_n \sigma} k_{r_m s_n}^{\nu(1)} |X_{r_m s_n}\rangle + \sum_{r_m s_n t_p z_q \sigma_1 \sigma_2} k_{r_m s_n t_p z_q}^{\nu(2)} |XX_{r_m s_n t_p z_q}\rangle + \dots \quad (5)$$

The above state can be characterized by a well-defined total angular momentum if each of its components belongs to the same subspace. For the sake of our discussion, we will label $|\Phi_\nu\rangle$ by the change of the angular momentum with respect to the HF ground state, denoted as Δm . In this case, the conservation of angular momentum throughout the correlated eigenstate requires $\Delta(n^{(1)} - m^{(1)}) = \Delta(q^{(2)} + p^{(2)} - n^{(2)} - m^{(2)})$, with the superscript representing the number of electron-hole pairs.

C. Absorption spectra and optical selection rules

We calculate the absorption spectrum of a photon with energy ω from Fermi's golden rule:

$$A(\omega) = \sum_{\nu, \nu'} W_\nu |\langle \Phi_{\nu'} | \hat{P}^+ | \Phi_\nu \rangle|^2 \delta(E_{\nu'} - E_\nu - \omega), \quad (6)$$

where the energies of the initial, $|\Phi_\nu\rangle$, and the final, $|\Phi_{\nu'}\rangle$, state participating in the absorption are E_ν and $E_{\nu'}$, respectively. The polarization operator $\hat{P}^+ = \sum_{r_m, s_n, \sigma} d(r_m, s_n) b_{r_m \sigma}^+ b_{s_n \sigma}$ adds a single-pair excitation while annihilating a photon. The coefficient W_ν describes the probability that the initial many-body state ν is occupied.

The dipole element $d(r_m, s_n)$ is calculated as described in our earlier work [70]. Expanding the HF quasiparticle states in terms of localized orbitals, one can show that electron-hole pairs can only be created on different angular momentum states by circularly polarized light:

$$d(r_m, s_n) = \langle r_m | \epsilon \cdot \vec{r} | s_n \rangle = C_{r,s} [1 - \delta_{m,n}], \quad (7)$$

where C is a numerical constant. Thus the dipole element dictates the emergence of optical selection rules where

transitions with $\Delta m = n - m = \pm 1$ correspond to circularly polarized photons with σ^\pm .

III. BAND-EDGE EXCITATIONS

In our graphene quantum dots, the $m = 1$ and 2 states constructed from the same set of orbitals are complex conjugates of each other, with degenerate eigenvalues [77]. In the semimetallic, weakly interacting electron regime with screening $\kappa > 2.3$ for C168 [70], the band edges are composed of degenerate $m = 1, 2$ valence and degenerate $m = 1, 2$ conduction-band states. In this section, we discuss multiexciton complexes built from the degenerate band-edge states. The effects of higher-energy conduction and lower-energy valence-band states will be considered in the following section.

A. Excitons

Let us briefly summarize our previous work [70] by discussing one-pair excitations and the formation of exciton states. Due to the degeneracy of levels, one can create in total eight single electron-hole pair excitations at the band edge without taking into account spin-flip excitations. Out of these eight, four belong to the $\Delta m = 0$ subspace, while the remaining 4 are distributed evenly between $\Delta m = \pm 1$ subspaces as depicted in Fig. 2. The exciton states are a linear combination of electron-hole pairs that block-diagonalize the interacting Hamiltonian, Eq. (4). Because of the angular-momentum selection rule, the states from the $\Delta m = 0$ subspace are not

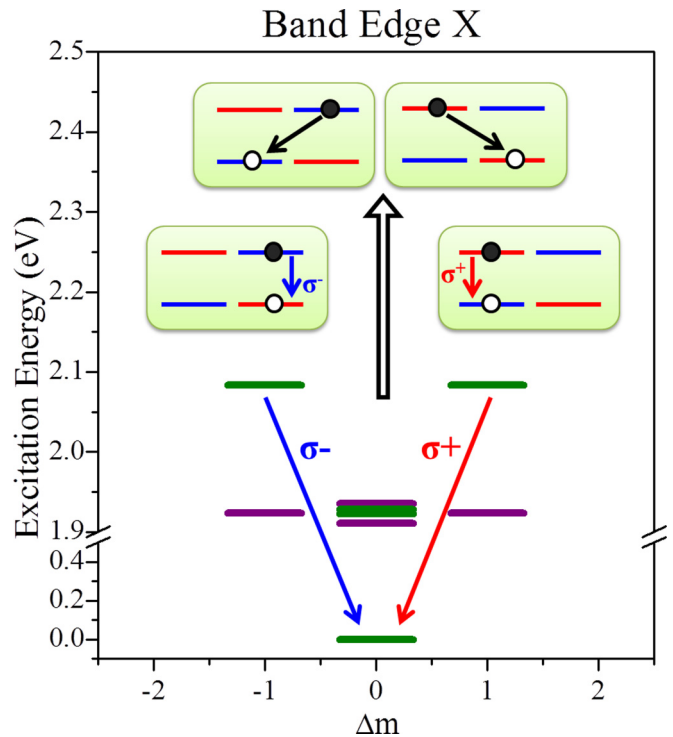


FIG. 2. (Color online) Ground state and the band-edge exciton spectrum normalized to ground-state energy. States are separated according to the change in angular momentum (electron m - hole m). Excitonic configurations contributing to each Δm set are shown in green boxes.

accessible via a single-photon process from the ground state, whether they are singlets or triplets. Out of the two states in each $\Delta m = \pm 1$ subspace, one is a singlet that can couple to the ground state through a single-photon process, while the other is a triplet and cannot couple to the ground state due to conservation of the total spin, as shown in Fig. 2.

B. Biexcitons

We now turn to two-pair excitations and the formation of biexciton states. There are 18 two-pair excitations that can be created at the band edge without spin flip. However, since we are interested in biexciton-exciton cascades, we will mainly study configurations that can couple optically to the bright excitons, namely the $\Delta m = \pm 1$ singlets. The Δm -labeled biexciton states are formed as linear combinations of two electron-hole pairs that block-diagonalize the interacting Hamiltonian, Eq. (4). To be able to distinguish the momentum of an electron-hole pair from that of an excitation, let us introduce Δm of excitons and biexcitons denoted by Δm_X and Δm_{XX} , respectively. Starting with either of the bright exciton configurations shown in Fig. 2, there are only two ways to create a biexciton state: by creating an electron-hole pair with $\Delta m = 1$ on an $(m = 1) - (m = 2)$ valence-conduction pair, or with $\Delta m = -1$ on an $(m = 2) - (m = 1)$ pair, as shown in Fig. 3(a). We note that it is not the total Δm_{XX} of the system but that of the excited electron-hole pairs that needs to be $\Delta m \neq 0$ to couple to light. For example, if we start with a $\Delta m_X = 1$ exciton, it can absorb light to become a $\Delta m_{XX} = 2$ or a $\Delta m_{XX} = 0$ biexciton.

A $\Delta m_{XX} = \pm 2$ biexciton at the band edge has both electron-hole pairs on the same conduction- and valence-band states as depicted in the right panel of Fig. 3(a). On the other hand, the biexciton configuration with $\Delta m_{XX} = 0$ will have each of its constituent carriers on a different band-edge state, as shown in the left panel of Fig. 3(a). This is the only $\Delta m_{XX} = 0$ XX configuration that can be directly created optically from *either* of the bright excitons. However, all $\Delta m_{XX} = 0$ biexciton states depicted in the figure will mix through Coulomb interactions.

The XX spectrum at the band edge is shown in the right panel of Fig. 3(b). The lowest $\Delta m_{XX} = 0$ band of biexciton states does not radiatively couple to any of the exciton states nor the ground state. The two $\Delta m_{XX} = 0$ states above the band only relax to triplet excitons. Next, the set of $\Delta m_{XX} = \pm 1$ biexcitons emits only to $\Delta m_X = 0$ excitons, thus they are not candidates for a cascade since the excitons they emit to are dark. As a result, at the band edge, there are only three states that emit to bright excitons, namely the $\Delta m_{XX} = \pm 2$ biexcitons and the highest energy $\Delta m_{XX} = 0$ biexciton. In emission, the $\Delta m = \Delta m_X - \Delta m_{XX}$ determines the polarization of the emitted photon; for $\Delta m = \pm 1$, the emitted photon will have a σ^\mp polarization.

IV. NUMERICAL RESULTS AND DISCUSSION

All numerical results presented in this paper are obtained assuming the dielectric constant $\kappa = 5.0$ and the tight-binding tunneling element $\tau = -4.2$ eV, in agreement with our previous work [70]. In CI calculations, we included up to

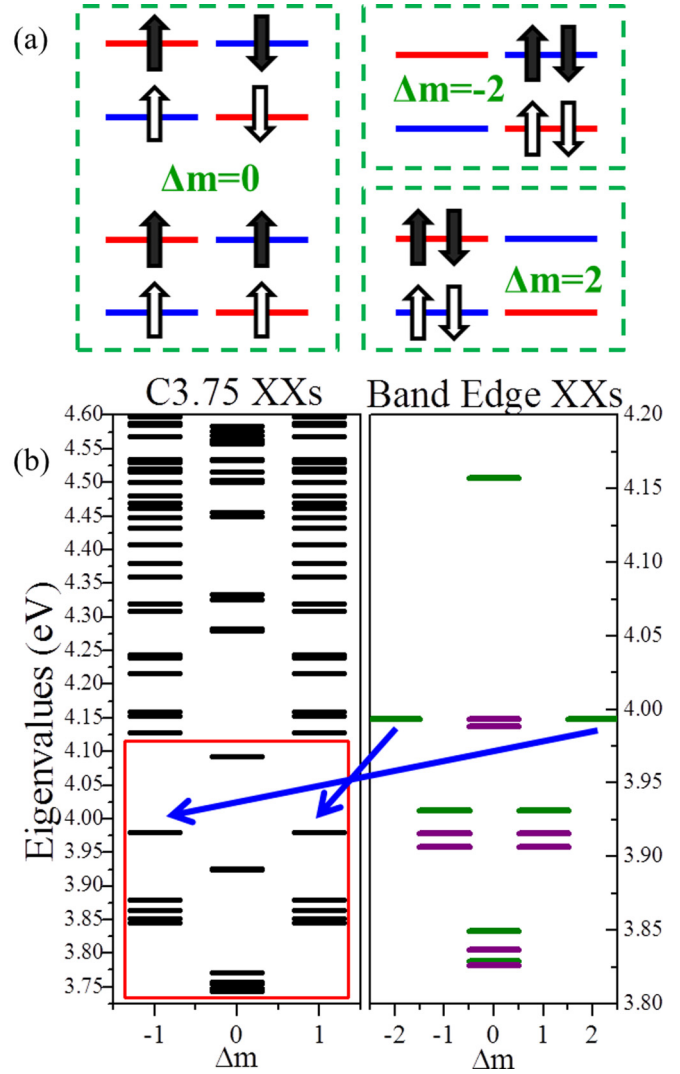


FIG. 3. (Color online) (a) Band-edge biexciton configurations with $\Delta m_{XX} = 0$ (left) and $\Delta m_{XX} = \pm 2$ (right) that are accessible from bright band-edge excitons. (b) The XX spectrum with a cutoff of $C = 3.75$ (left) and $v2c2$ (right). Blue arrows show mapping of the $\Delta m = \pm 2$ subspace onto $\Delta m = \mp 1$.

four electron-hole pairs leading to a Hilbert space of up to 0.8×10^6 configurations.

A. Convergence of the biexciton spectrum

In the preceding section, we discussed the XX spectrum at the band edge. We now discuss how this spectrum changes when electrons and holes can scatter into excited orbitals. Due to the size of our configuration space, we reduce the number of states taken into account in several steps. After calculating the HF quasiparticle states and energies, we organize the CI subspace to systematically increase the number of excited states away from the band edge. Since we are also interested in the Auger processes, the CI subspace is chosen to include HF states allowing Auger coupling between an excited exciton (X^*) and a band edge XX , as illustrated in Fig. 4. Starting with a band-edge biexciton, one of the electron-hole pairs can recombine giving the excess energy to the remaining

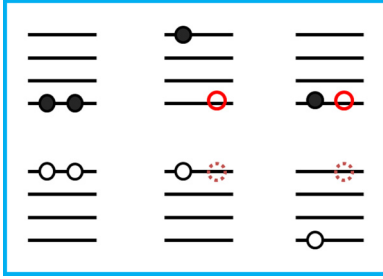


FIG. 4. (Color online) Auger coupling at the band edge. Starting with a biexciton at the band edge (left), an electron-hole pair can recombine to promote the electron (hole) higher (lower) in energy. Thus the biexciton state and the excited excitons of the same energy may couple, leading to decay of XX .

electron-hole pair, exciting the electron up or the hole down by an energy equivalent to the band gap, E_g . Thus, as shown in Fig. 4, we need to include all HF states within the window of $3E_g$ from the center of the band gap to allow Auger coupling of the band edge XX 's to excited X^* states.

The $3E_g$ CI window corresponds to 15 valence- and 23 conduction-band states. Even though one can technically create up to 30 electron-hole pair configurations within this window, even to create a $3X$ configuration, one needs more than three times the band-gap energy, which is significantly greater than the energy range in which we are interested.

Thus, we start by restricting the maximum number of excitations to two. However, even a space with $GS + X + XX$ constitutes more than 1.7×10^6 configurations.

Within the $3E_g$ window of HF quasiparticle states, one can create biexcitons with energies up to six times that of the band gap by creating electron-hole pairs from the lowest valence and the highest conduction states taken within the CI window. While keeping all excitons that can be created within this window, we introduce a cutoff of $E_{XX} \leq CE_g$ for biexcitons, with C being an adjustable coefficient.

The left panel of Fig. 3(b) shows the biexciton levels calculated with the $C = 3.75$ cutoff for their energies. Even though, at the band edge, we treated the $\Delta m = \pm 2$ configurations as if they each had their own angular-momentum separated subspace, it is not the case once we include HF states beyond the band edge. Inclusion of the $m = 0$ higher-energy states dictates that the change in the angular-momentum space $\Delta m = \pm 2$ maps onto $\Delta m = \mp 1$, respectively. This mapping is shown by blue arrows for the $\Delta m_{XX} = \pm 2$ band-edge biexciton states in Fig. 3(b).

In Fig. 5, we illustrate the convergence of the XX excitation energies, $E_{\text{exc}}^{XX} = E_{XX} - E_{\text{GS}}$, in the CI subspace with $GS + X + XX$. Here, E_{XX} and E_{GS} are, respectively, the XX and GS energies. The labeling of the horizontal axis is as follows. The label $vMcM$ corresponds to a CI subspace constructed from the first M valence and conduction states. The rest of the labels denote the choice of the cutoff parameter C for the case in which all $GS + X$ configurations on 15 valence and 23 conduction states are taken into account while restricting the number of XX 's as described above. Since all classes of excitations, GS , X , and XX , converge at different rates, we track the convergence of the eigenvalues instead of excitation energies from the ground state. One can extrapolate converged

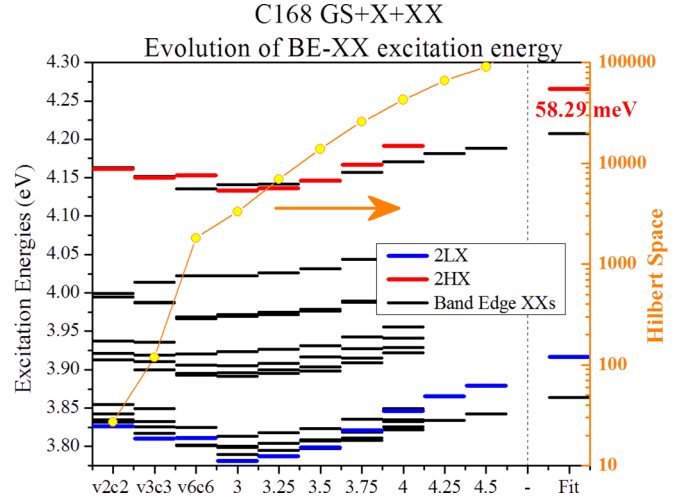


FIG. 5. (Color online) Evolution of the highest and lowest band-edge XX energies and twice the lowest (highest) -exciton energies with an increasing number of configurations included within a subspace of $GS + X + XX$. The fit for $N_{\text{conf}} \rightarrow \infty$ is shown in the right column. The yellow dots correspond to the size of the Hilbert space. The HX for $C = 4.25$ and 4.50 were not calculated due to size limitations. $2LX$ corresponds to $2 \times$ lowest triplet exciton excitation energy, which is depicted in the figure to guide the eye as the lower bound. $2HX$ is the excitation energy of $2 \times$ degenerate singlet excitons, and thus the separation between the highest XX excitation energy and the red line corresponds to the HXX binding energy.

eigenvalues by plotting the calculated values as a function of $1/N_{\text{conf}}$, where N_{conf} is the number of configurations included in each subspace, and tracking the trend to $N_{\text{conf}} \rightarrow \infty$. The fits for the lowest and highest band-edge biexciton and exciton excitation energies, E_{exc}^{XX} and $2E_{\text{exc}}^X$, are plotted at the very right column of Fig. 5, where the exciton excitation energies are defined as $E_{\text{exc}}^X = E_X - E_{\text{GS}}$.

B. Biexciton binding

Experimentally, the biexciton binding energy is extracted from the emission spectra of XX 's and X 's and it is defined as $E_b^{XX} = E_{\text{exc}}^{X_1} + E_{\text{exc}}^{X_2} - E_{\text{exc}}^{XX}$. The first two terms are the energies of the two constituent excitons, counted separately, while the third term is the energy of the biexciton complex. The sign of E_b^{XX} can be positive or negative, corresponding to excitons attracting (binding) or repelling (unbinding) each other, respectively. It is also an indicator of the degree of correlation, which is measured by the number of two-electron-hole configurations contributing to the XX state. Looking at the last column of Fig. 5, we see that both the lowest and the highest XX states are bound in the Hilbert space, which includes GS , X , and XX excitations. Approaching convergence, there are around 10^6 configurations, and the XX states become increasingly correlated.

We further investigated the effects of size and shape on the binding energy by computing binding energies for different shapes of CGQDs at the $v2c2$ level with inclusion of up to $4X$. As expected, the binding energy increases inversely with the size of the C_3 symmetric quantum dots. However, as soon as we break the C_3 symmetry, even if we increase the quantum dot

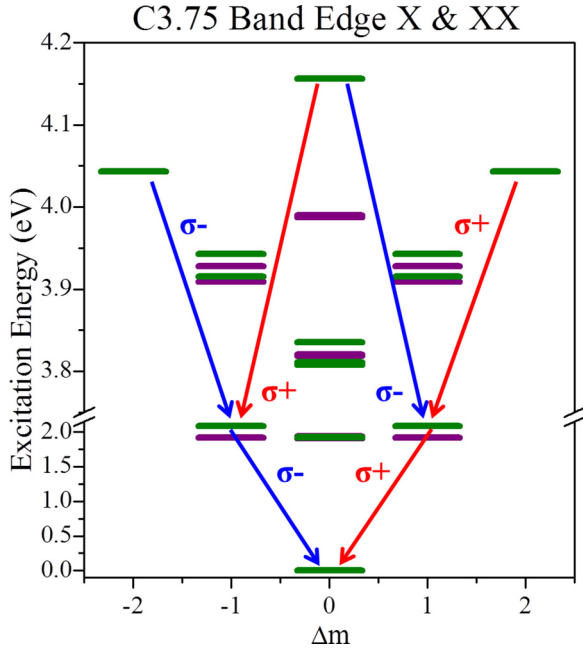


FIG. 6. (Color online) Band-edge excitons and biexcitons showing possible XX - X cascade routes. Green and purple are singlet and triplet states, respectively.

size, the binding energies of both the lowest and the highest XX increase significantly. The sign of the binding energy, however, does not seem to be affected by the size or the shape of the quantum dot.

C. Biexciton-exciton cascade

The band edge XX 's that can contribute to the XX - X cascade are the highest $\Delta m = 0$ XX and the two $\Delta m = \pm 2$ XX 's, depicted in Fig. 6.

In the XX - X cascade, both electron-hole pairs of the biexciton recombine, each emitting a photon. If we prepare the C_3 symmetric graphene quantum dot in the state of the highest band edge $\Delta m_{XX} = 0$ biexciton, the entangled Bell state of the two photons generated in its radiative recombination will be

$$|\psi\rangle = \frac{1}{\sqrt{2}}(|\sigma^- \sigma^+\rangle + |\sigma^- \sigma^+\rangle). \quad (8)$$

This process is depicted in Fig. 6. Starting from the highest band edge XX , one can choose either the left or the right path emitting a σ^+ - or σ^- -polarized photon. The second photon emitted in this process will have the polarization opposite to the first photon.

If the CGQD is prepared in a superposition of the $\Delta m_{XX} = \pm 2$ biexcitons, shown in Fig. 6, the photons emerging from the recombination process will be polarization-entangled, and their two-photon Bell state will be expressed as

$$|\psi\rangle = \frac{1}{\sqrt{2}}(|\sigma^- \sigma^- \rangle + |\sigma^+ \sigma^+ \rangle). \quad (9)$$

If, on the other hand, the CGQD is prepared in a state with a specific angular momentum $\Delta m_{XX} = 2$ or -2 , then the state of the photons will collapse to a certain polarization, $p = \pm$, $|\psi\rangle = |\sigma^p \sigma^p\rangle$, and the entanglement will be destroyed.

D. Auger processes and XX spectral function

To understand the Auger processes between the highest band edge XX and the highly excited excitons, we examine the spectral function of the biexciton interacting with the excited exciton states. Its calculation involves two steps. First, one needs to calculate separately the eigenstates and eigenvalues of the mixed system ($GS + X + XX$) and the eigenstates and eigenvalues of the system in which only the configurations with two electron-hole pairs are included (the ‘‘conserved’’ system). After exact diagonalization of the Hamiltonian for the mixed system, we obtain the eigenfunctions in the form of (5). As for the system restricted to the two-pair excitations, the exact diagonalization procedure produces the following eigenfunctions [79]:

$$|XX\rangle_\eta = \sum_{i,j,k,l} \sum_{\sigma_1,\sigma_2} k_{ijkl}^{(2)} |XX_{ijkl}\rangle. \quad (10)$$

In our calculations, we restrict our basis in the same manner for both $|XX\rangle_\eta$ and Φ_ν as described in Sec. IV A.

Once we have the eigenfunctions and the eigenvalues of both mixed and conserved systems, to quantify the degree of mixing between a biexciton state $|XX\rangle_\nu$ and the rest of the mixed system, we define the spectral function $A_{\eta,XX}(\nu)$ as

$$A_{\eta,XX}(E) = \sum_\nu |{}_\eta\langle XX|\Phi_\nu\rangle|^2 \delta(E_\nu - E). \quad (11)$$

This function is the projection of a conserved biexciton state, XX_η , onto the states of the mixed system [79]. In the weak XX - X coupling limit, the spectral function will approach $A_{\eta,XX}(\nu) \rightarrow 1$ for ν corresponding to XX_η . The spectral function of the HXX state of the conserved system is shown in Fig. 7. The greatest $A_{HXX}(\nu)$ peak with a value of 0.85, describing the HXX interacting with excited X states, shows that the XX is stable against Auger recombination. The

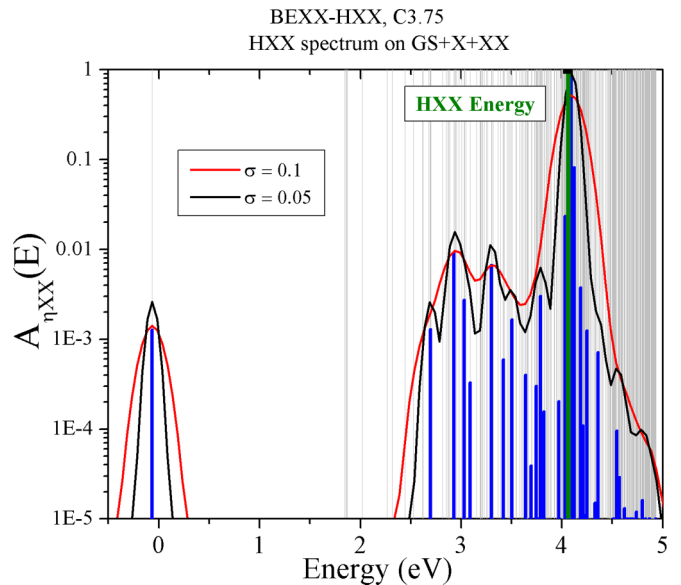


FIG. 7. (Color online) Spectral function of the highest biexciton state HXX . Red and blue curves are for different Gaussian broadenings. The green peak corresponds to the HXX energy from the conserved system.

inverse of the width of the spectral function defines the Auger lifetime. As in semiconductor nanocrystals [79], the calculated Auger lifetime is significantly higher than the experimentally measured one [47]. The origin of this discrepancy remains to be determined.

V. CONCLUSIONS

In this paper, we presented a microscopic theory of biexcitons in graphene quantum dots. The single-particle properties were described in the tight-binding model, and electron-electron interactions were included using the Hartree-Fock and configuration-interaction methods. The many-body ground, exciton, and biexciton states were expanded in a basis of a finite number of electron-hole pair excitations from

the Hartree-Fock ground state and determined numerically using exact diagonalization techniques. The biexciton band characteristic of the degenerate bottom of the conduction band and the top of the valence band was predicted. The relevant XX state and two corresponding degenerate exciton (X) states were identified for the generation of an $XX-X$ cascade, a source of polarization-entangled photon pairs. The Auger process relevant to the XX contributing to the cascade was determined. These results show that graphene quantum dots are potentially highly tunable sources of entangled photon pairs.

ACKNOWLEDGMENTS

I.O. and P.H. thank NSERC for support. The authors thank J. McGuire for discussions.

-
- [1] P. R. Wallace, *Phys. Rev.* **71**, 622 (1947).
- [2] K. S. Novoselov, A. K. Geim, S. V. Morozov, D. Jiang, Y. Zhang, S. V. Dubonos, I. V. Grigorieva, and A. A. Firsov, *Science* **306**, 666 (2004).
- [3] K. S. Novoselov, A. K. Geim, S. V. Morozov, D. Jiang, M. I. Katsnelson, I. V. Grigorieva, S. V. Dubonos, and A. A. Firsov, *Nature (London)* **438**, 197 (2005).
- [4] Y. B. Zhang, Y. W. Tan, H. L. Stormer, and P. Kim, *Nature (London)* **438**, 201 (2005).
- [5] S. Y. Zhou, G. H. Gweon, J. Graf, A. V. Fedorov, C. D. Spataru, R. D. Diehl, Y. Kopelevich, D. H. Lee, S. G. Louie, and A. Lanzara, *Nat. Phys.* **2**, 595 (2006).
- [6] A. H. Castro Neto, F. Guinea, N. M. R. Peres, K. S. Novoselov, and A. K. Geim, *Rev. Mod. Phys.* **81**, 109 (2009).
- [7] A. K. Geim and K. S. Novoselov, *Nat. Mater.* **6**, 183 (2007).
- [8] A. K. Geim, *Science* **324**, 1530 (2009).
- [9] C. Faugeras, M. Amado, P. Kossacki, M. Orlita, M. Kühne, A. A. L. Nicolet, Yu. I. Latyshev, and M. Potemski, *Phys. Rev. Lett.* **107**, 036807 (2011).
- [10] D. M. Hoffman, P. C. Eklund, R. E. Heinz, P. Hawrylak, and K. R. Subbaswamy, *Phys. Rev. B* **31**, 3973 (1985).
- [11] J. Blinowski, N. H. Hau, C. Rigaux, J. P. Vieren, R. Le Toullec, G. Furdin, A. Herold, and J. Melin, *J. Phys. (Paris)* **41**, 47 (1980).
- [12] M. L. Sadowski, G. Martinez, M. Potemski, C. Berger, and W. A. de Heer, *Phys. Rev. Lett.* **97**, 266405 (2006).
- [13] M. Orlita, C. Faugeras, P. Plochocka, P. Neugebauer, G. Martinez, D. K. Maude, A. L. Barra, M. Sprinkle, C. Berger, W. A. de Heer, and M. Potemski, *Phys. Rev. Lett.* **101**, 267601 (2008).
- [14] R. R. Nair, P. Blake, A. N. Grigorenko, K. S. Novoselov, T. J. Booth, T. Stauber, N. M. R. Peres, and A. K. Geim, *Science* **320**, 1308 (2008).
- [15] F. Wang, Y. B. Zhang, C. S. Tian, C. Girit, A. Zettl, M. Crommie, and Y. R. Shen, *Science* **320**, 206 (2008).
- [16] Z. Q. Li, E. A. Henriksen, Z. Jiang, Z. Hao, M. C. Martin, P. Kim, H. L. Stormer, and D. N. Basov, *Nat. Phys.* **4**, 532 (2008).
- [17] K. F. Mak, M. Y. Sfeir, Y. Wu, C. H. Lui, J. A. Misewich, and T. F. Heinz, *Phys. Rev. Lett.* **101**, 196405 (2008).
- [18] M. Koshino and T. Ando, *Phys. Rev. B* **77**, 115313 (2008).
- [19] T. Mueller, F. N. A. Xia, and P. Avouris, *Nat. Photon.* **4**, 297 (2010).
- [20] L. Yang, J. Deslippe, C. H. Park, M. L. Cohen, and S. G. Louie, *Phys. Rev. Lett.* **103**, 186802 (2009).
- [21] T. Yamamoto, T. Noguchi, and K. Watanabe, *Phys. Rev. B* **74**, 121409 (2006).
- [22] A. D. Guclu and P. Hawrylak, *Phys. Rev. B* **87**, 035425 (2013).
- [23] Z. Z. Zhang, K. Chang, and F. M. Peeters, *Phys. Rev. B* **77**, 235411 (2008).
- [24] A. D. Guclu, P. Potasz, and P. Hawrylak, *Phys. Rev. B* **82**, 155445 (2010).
- [25] A. D. Guclu, P. Potasz, M. Korkusinski, and P. Hawrylak, *NanoScience and Technology* (Springer, Berlin, Heidelberg, 2014).
- [26] W. Sheng, M. Korkusinski, A. D. Guclu, M. Zielinski, P. Potasz, E. S. Kadantsev, O. Voznyy, P. Hawrylak, *Front. Phys.* **7**, 328 (2012).
- [27] J. S. Bunch, Y. Yaish, M. Brink, K. Bolotin, and P. L. McEuen, *Nano Lett.* **5**, 287 (2005).
- [28] T. Ihn, S. Gustavsson, U. Gasser, B. Kung, T. Muller, R. Schleser, M. Sigrist, I. Shorubalko, R. Leturcq, and K. Ensslin, *Solid State Commun.* **149**, 1419 (2009).
- [29] L. A. Ponomarenko, F. Schedin, M. I. Katsnelson, R. Yang, E. W. Hill, K. S. Novoselov, and A. K. Geim, *Science* **320**, 356 (2008).
- [30] B. Wunsch, T. Stauber, and F. Guinea, *Phys. Rev. B* **77**, 035316 (2008).
- [31] J. Wurm, A. Rycerz, I. Adagideli, M. Wimmer, K. Richter, and H. U. Baranger, *Phys. Rev. Lett.* **102**, 056806 (2009).
- [32] F. Libisch, C. Stampfer, and J. Burgdorfer, *Phys. Rev. B* **79**, 115423 (2009).
- [33] J. Akola, H. P. Heiskanen, and M. Manninen, *Phys. Rev. B* **77**, 193410 (2008).
- [34] M. Ezawa, *Phys. Rev. B* **81**, 201402 (2010).
- [35] P. Potasz, A. D. Guclu, and P. Hawrylak, *Phys. Rev. B* **81**, 033403 (2010).
- [36] P. Potasz, A. D. Guclu, and P. Hawrylak, *Phys. Rev. B* **82**, 075425 (2010).
- [37] B. Yuma, S. Berciaud, J. Besbas, J. Shaver, S. Santos, S. Ghosh, R. B. Weisman, L. Cognet, M. Gallart, M. Ziegler, B. Hönerlage, B. Lounis, and P. Gilliot, *Phys. Rev. B* **87**, 205412 (2013).

- [38] K. Watanabe and K. Asano, *Phys. Rev. B* **83**, 115406 (2011).
- [39] D. Kammerlander, D. Prezzi, G. Goldoni, E. Molinari, and U. Hohenester, *Phys. Rev. Lett.* **99**, 126806 (2007).
- [40] T. G. Pedersen, K. Pedersen, H. D. Cornean, and P. Duclos, *Nano Lett.* **5**, 291 (2005).
- [41] D. J. Styers-Barnett, S. P. Ellison, B. P. Mehl, B. C. Westlake, R. L. House, C. Park, K. E. Wise, and J. M. Papanikolas, *J. Phys. Chem. C* **112**, 4507 (2008).
- [42] H. Zhao and S. Mazumdar, *Phys. Rev. Lett.* **93**, 157402 (2004).
- [43] J. M. Leng, S. Jeglinski, X. Wei, R. E. Benner, Z. V. Vardeny, F. Guo, and S. Mazumdar, *Phys. Rev. Lett.* **72**, 156 (1994).
- [44] H. Zhao, S. Mazumdar, C.-X. Sheng, M. Tong, and Z. V. Vardeny, *Phys. Rev. B* **73**, 075403 (2006).
- [45] V. I. Klimov, D. W. McBranch, N. Barashkov, and J. Ferraris, *Phys. Rev. B* **58**, 7654 (1998).
- [46] M. A. Pasquinelli and D. Yaron, *J. Chem. Phys.* **118**, 8082 (2003).
- [47] C. Sun, F. Figge, J. A. McGuire, Q. Li, and L.-S. Li, *Phys. Rev. Lett.* **113**, 107401 (2014).
- [48] C. Sun, F. Figgie, I. Ozfidan, M. Korkusinski, X. Yan, L.-S. Li, P. Hawrylak, and J. A. McGuire (unpublished).
- [49] L. C. Campos, V. R. Manfrinato, J. D. Sanchez-Yamagishi, J. Kong, and P. Jarillo-Herrero, *Nano Lett.* **9**, 2600 (2009).
- [50] M. Ezawa, *Phys. Rev. B* **76**, 245415 (2007).
- [51] J. Fernandez-Rossier and J. J. Palacios, *Phys. Rev. Lett.* **99**, 177204 (2007).
- [52] W. L. Wang, S. Meng, and E. Kaxiras, *Nano Lett.* **8**, 241 (2008).
- [53] J. Jung and A. H. MacDonald, *Phys. Rev. B* **79**, 235433 (2009).
- [54] A. D. Guclu, P. Potasz, O. Voznyy, M. Korkusinski, and P. Hawrylak, *Phys. Rev. Lett.* **103**, 246805 (2009).
- [55] P. Potasz, A. D. Guclu, A. Wojs, and P. Hawrylak, *Phys. Rev. B* **85**, 075431 (2012).
- [56] O. Voznyy, A. D. Guclu, P. Potasz, and P. Hawrylak, *Phys. Rev. B* **83**, 165417 (2011).
- [57] P. Potasz, A. D. Guclu, O. Voznyy, J. A. Folk, and P. Hawrylak, *Phys. Rev. B* **83**, 174441 (2011).
- [58] O. Benson, C. Santori, M. Pelton, and Y. Yamamoto, *Phys. Rev. Lett.* **84**, 2513 (2000).
- [59] N. Akopian, N. H. Lindner, E. Poem, Y. Berlatzky, J. Avron, D. Gershoni, B. D. Gerardot, and P. M. Petroff, *Phys. Rev. Lett.* **96**, 130501 (2006).
- [60] M. Shirane, Y. Igarashi, Y. Ota, M. Nomura, N. Kumagai, S. Ohkouchi, A. Kirihaara, S. Ishida, S. Iwamoto, S. Yoroazu, and Y. Arakawa, *Physica E* **42**, 2563 (2010).
- [61] M. Muller, S. Bounouar, K. D. Jons, M. Glassl, and P. Michler, *Nat. Photon.* **8**, 224 (2014).
- [62] A. H. Trojnar, E. S. Kadantsev, M. Korkusinski, and P. Hawrylak, *Phys. Rev. B* **84**, 245314 (2011).
- [63] M. Bayer, G. Ortner, O. Stern, A. Kuther, A. A. Gorbunov, A. Forchel, P. Hawrylak, S. Fafard, K. Hinzer, T. L. Reinecke, S. N. Walck, J. P. Reithmaier, F. Klopff, and F. Schafer, *Phys. Rev. B* **65**, 195315 (2002).
- [64] R. M. Stevenson, R. J. Young, P. Atkinson, K. Cooper, D. A. Ritchie, and A. J. Shields, *Nature* **439**, 179 (2006).
- [65] M. E. Reimer, D. Dalacu, J. P. Poole, and R. L. Williams, *J. Phys: Conf. Ser.* **210**, 012019 (2010).
- [66] R. J. Young, R. M. Stevenson, P. Atkinson, K. Cooper, D. A. Ritchie, and A. J. Shields, *New J. Phys.* **8**, 29 (2006).
- [67] M. E. Reimer, M. P. van Kouwen, M. H. van Weert, E. P. Bakkers, L. P. Kouwenhoven, and V. Zwiller, *Nano Lett.* **11**, 645 (2011).
- [68] S. V. Goupalov, E. L. Ivchenko, and A. V. Kavokin, *JETP* **86**, 388 (1998).
- [69] S. V. Goupalov, E. L. Ivchenko, and A. V. Kavokin, *Superlatt. Microstruct.* **23**, 1205 (1998).
- [70] I. Ozfidan, M. Korkusinski, A. D. Guclu, J. A. McGuire, and P. Hawrylak, *Phys. Rev. B* **89**, 085310 (2014).
- [71] X. Yan, X. Cui, and L. Li, *J. Am. Chem. Soc.* **132**, 5944 (2010).
- [72] X. Yan, X. Cui, B. Li, and L. Li, *Nano Lett.* **10**, 1869 (2010).
- [73] M. L. Mueller, X. Yan, J. A. McGuire, and L. Li, *Nano Lett.* **10**, 2679 (2010).
- [74] X. Yan, B. Li, X. Cui, Q. Wei, K. Tajima, and L. Li, *J. Phys. Chem. Lett.* **2**, 1119 (2011).
- [75] X. Yan, B. Li, and L. Li, *Acc. Chem. Res.* **46**, 2254 (2013).
- [76] S. Schumacher, *Phys. Rev. B* **83**, 081417 (2011).
- [77] A. V. Rozhkov and F. Nori, *Phys. Rev. B* **81**, 155401 (2010).
- [78] I. Puerto Gimenez, M. Korkusinski, and P. Hawrylak, *Phys. Rev. B* **76**, 075336 (2007).
- [79] M. Korkusinski, O. Voznyy, and P. Hawrylak, *Phys. Rev. B* **84**, 155327 (2011).